PlexinA1 is a new Slit receptor and mediates axon guidance function of Slit C-terminal fragments

Céline Delloye-Bourgeois, Arnaud Jacquier, Camille Charoy, Florie Reynaud, Homaira Nawabi, Karine Thoinet, Karine Kindbeiter, Yutaka Yoshida, Yvrick Zagar, Youxin Kong, et al.

nature neuroscience

PlexinA1 is a new Slit receptor and mediates axon guidance function of Slit C-terminal fragments

Céline Delloye-Bourgeois[1], Arnaud Jacquier[1], Camille Charoy[1], Florie Reynaud[1], Homaira Nawabi[1], Karine Thoinet[1], Karine Kindbeiter[1], Yutaka Yoshida[2], Yvrick Zagar[3–5], Youxin Kong[6], Yvonne E Jones[6], Julien Falk[1], Alain Chédotal[3–5] & Valérie Castellani[1]

Robo-Slit and Plexin-Semaphorin signaling participate in various developmental and pathogenic processes. During commissural axon guidance in the spinal cord, chemorepulsion by Semaphorin3B and Slits controls midline crossing. Slit processing generates an N-terminal fragment (SlitN) that binds to Robo1 and Robo2 receptors and mediates Slit repulsive activity, as well as a C-terminal fragment (SlitC) with an unknown receptor and bioactivity. We identified PlexinA1 as a Slit receptor and found that it binds the C-terminal Slit fragment specifically and transduces a SlitC signal independently of the Robos and the Neuropilins. PlexinA1–SlitC complexes are detected in spinal cord extracts, and *ex vivo*, SlitC binding to PlexinA1 elicits a repulsive commissural response. Analysis of various ligand and receptor knockout mice shows that PlexinA1-Slit and Robo-Slit signaling have complementary roles during commissural axon guidance. Thus, PlexinA1 mediates both Semaphorin and Slit signaling, and Slit processing generates two active fragments, each exerting distinct effects through specific receptors.

In the developing nervous system, axonal navigation is controlled by multiple extracellular cues[1]. This complex guidance information is transduced within the axonal growth cone through a variety of signaling cascades initiated by specialized cell surface receptors and leading to growth cone cytoskeleton reorganization[2]. Midline crossing by spinal commissural axons is a model that is well suited to investigate axon guidance mechanisms[3,4]. Remarkably, the sensitivity of commissural growth cones is set in time and space, so that during their navigation they are initially attracted toward the ventral floor plate (FP), where they cross the midline and gain sensitivity to local repellents, which steer them away from the FP toward their next target[5]. How such temporal and spatial regulations are set remains obscure. The Semaphorin Sema3B is an important midline cue in vertebrates[6,7] whose repulsive activity is triggered through suppression of the processing of its signaling co-receptor, PlexinA1 (refs. 7,8). Slits are other major midline repellents[9–12]. The vertebrate FP expresses all three mammalian Slits (Slit1–Slit3), which act synergistically[12,13]. Slit2, and probably Slit1, are processed into a N-terminal fragment (Slit2N, 140 kDa) and a C-terminal fragment (Slit2C, 55–60 kDa) both *in vitro* and *in vivo* through an unknown proteolytic process. So far, almost all of the various Slit signaling activities have been attributed to its N-terminal fragment, although some reports have indicated that full-length Slits (Slit-FL) are active as well[14–16]. In contrast, the C-terminal Slit fragments do not have any known biological activity. The Roundabout (Robo) receptors have been found to mediate all Slit activities reported so far, and they bind both Slit-FL and SlitN. Nevertheless, the existence of an unidentified additional receptor for Slits has been suggested in part by the finding that deficiencies in both Robo1 and Robo2 and in all Slits (Slit1, Slit2 and Slit3) do not result in strictly similar defects. Robo abrogation leads to a much lower rate of guidance errors—midline recrossing and stalling—than does Slit abrogation[17]. Here we report the identification of a new receptor for Slits, PlexinA1, and characterize the bioactivity of Slit C-terminal fragments during commissural axon guidance.

RESULTS

PlexinA1 deficiency is reminiscent of Robo–Slit loss

To determine whether PlexinA1 could have Sema3B-independent functions during commissural axon guidance, we first analyzed commissural axon trajectories in *PlexinA1* (*Plxna1*)-null mutant mice. We inserted fast 1,1′-dilinoleyl-3,3,3′,3′-tetramethylindocarbocyanine, 4-chlorobenzenesulfonate (DiI) crystals into the dorsal part of spinal cord open-book preparations containing commissural neurons from embryonic day (E) 12.5 mice (**Supplementary Fig. 1**). As reported previously, we observed crossing and post-crossing defects consisting mainly of stalling and aberrant turning in 78% of *PlexinA1*-mutant mice ($Plxna1^{-/-}$) compared to 30% and 68% of mice with wild-type (WT, $Plxna1^{+/+}$) and heterozygous ($Plxna1^{+/-}$) *PlexinA1*, respectively (number of crystals/number of embryos: 81/8 for $Plxna1^{+/+}$, 82/8 for $Plxna1^{+/-}$ and 103/10 for $Plxna1^{-/-}$) (**Fig. 1a**,**b** and ref. 7). We observed all of these defects in *Sema3B*-null mice as well, reflecting the contribution of Sema3B-PlexinA1 signaling at the midline[7]. However, in 17% of *PlexinA1*-null embryos, some commissural axons reached the FP and turned back toward the ipsilateral side,

[1]University of Lyon, University Claude Bernard Lyon 1, CGphiMC UMR CNRS 5534, Lyon, France. [2]Division of Developmental Biology, Cincinnati Children's Hospital Medical Center, Cincinnati, Ohio, USA. [3]INSERM, UMRS_U968, Institut de la Vision, Paris, France. [4]Sorbonne Universités, Université Pierre et Marie Curie (UPMC) University of Paris 06, Institut de la Vision, Paris, France. [5]CNRS, UMR_7210, Paris, France. [6]Wellcome Trust Centre for Human Genetics, University of Oxford, Oxford, UK. Correspondence should be addressed to V.C. (valerie.castellani@univ-lyon1.fr).

Received 4 September; accepted 12 November; published online 8 December 2014; doi:10.1038/nn.3893

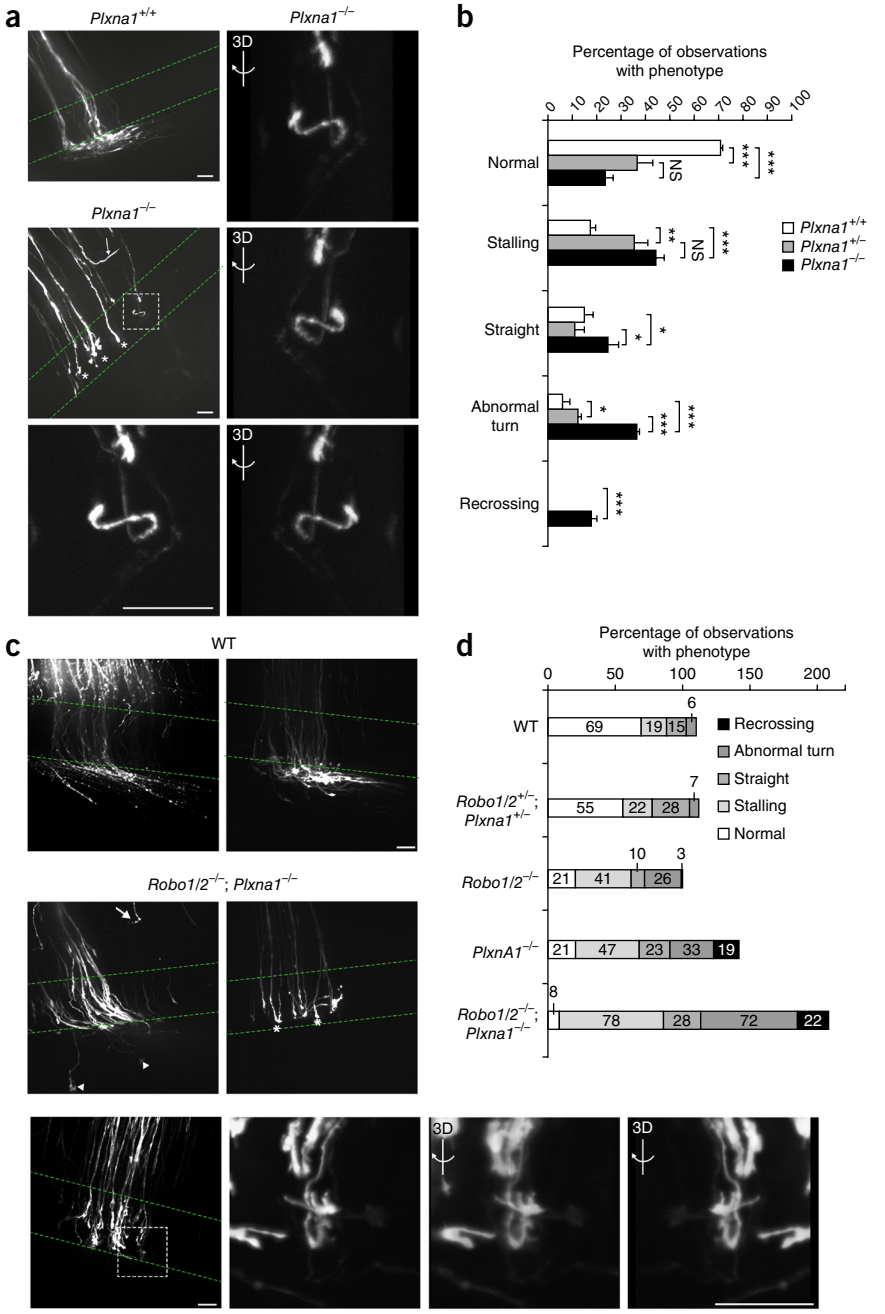

Figure 1 *Plxna1*, *Robo1* and *Robo2* triple deficiency recapitulates midline guidance defects induced by loss of *Slit1*, *Slit2* and *Slit3*. (**a**) Microphotographs illustrating defective trajectories in *Plxna1*$^{-/-}$ embryos: stalling (*), premature turning (arrow) and recrossing (dashed square). The images on the right show a three-dimensional reconstruction of the recrossing. Scale bars, 25 µm. Dashed green lines underline the FP. (**b**) Phenotypic analysis of WT (*Plxna1*$^{+/+}$; $n = 8$ embryos, 81 crystals), heterozygous (*Plxna1*$^{+/-}$; $n = 8$ embryos, 82 crystals) and null (*Plxna1*$^{-/-}$; $n = 10$ embryos, 103 crystals) embryos. Data are shown as the mean ± s.e.m.; normal in *Plxna1*$^{+/-}$ compared to *Plxna1*$^{-/-}$: $P = 0.075$; stalling in *Plxna1*$^{+/+}$ compared to *Plxna1*$^{+/-}$: $P = 0.0028$; stalling in *Plxna1*$^{+/-}$ compared to *Plxna1*$^{-/-}$: $P = 0.141$; straight in *Plxna1*$^{+/+}$ compared to *Plxna1*$^{-/-}$: $P = 0.029$; straight in *Plxna1*$^{+/-}$ compared to *Plxna1*$^{-/-}$: $P = 0.010$; straight in *Plxna1*$^{+/-}$ compared to *Plxna1*$^{-/-}$: $P = 0.010$. *$P < 0.05$, **$P < 0.05$, ***$P < 0.001$, Student's *t* test. NS, not significant. (**c**) Microphotographs of DiI-labeled commissural tracts in WT embryos and misrouting phenotypes in *Robo1*, *Robo2* and *Plxna1* triple-null embryos (*Robo1/2*$^{-/-}$; *Plxna1*$^{-/-}$) with stalling (*), premature turning (arrow), abnormal turning (arrowheads) and recrossing (dashed square). Scale bars, 25 µm. (**d**) Quantitative analysis of WT ($n = 10$ embryos, 101 crystals), triple heterozygous (*Robo1*$^{+/-}$; *Robo2*$^{+/-}$ (*Robo1/2*$^{+/-}$); *Plxna1*$^{+/-}$; $n = 5$ embryos, 58 crystals), *Robo1* and *Robo2* null (*Robo1/2*$^{-/-}$; $n = 3$ embryos, 28 crystals), *Plxna1*-null (*Plxna1*$^{-/-}$; $n = 13$ embryos, 134 crystals) and triple *Robo1*, *Robo2* and *Plxna1* null (*Robo1/2*$^{-/-}$; *Plxna1*$^{-/-}$; $n = 3$ embryos, 36 crystals) embryos. The percentages of DiI crystals with each phenotype are indicated on the graph for each class of phenotype.

thus recrossing the FP (**Fig. 1a**,**b**). We did not observe this phenomenon in either the *Sema3B*-null or WT mice, thereby supporting Sema3B-independent role(s) of PlexinA1 to prevent midline recrossing.

To further assess this possibility, we electroporated GFP and glycosylphosphatidylinisotol (GPI)-anchored PlexinA acting as a dominant negative for PlexinA (PlexinA-DN)[18] or a control empty vector into chick neural tubes. We observed GFP$^+$ commissural axon trajectories in open-book preparations from these chicks 48 h after electroporation (**Supplementary Fig. 2a**). FP stalling and abnormal turning were increased by 175% in the PlexinA-DN condition as compared to the controls (number of fields/number of embryos: 107/8 for embryos electroporated with GFP and empty vector; and 112/9 for embryos electroporated with GFP and PlexinA-DN) (**Supplementary Fig. 2a**,**b**). Notably, we observed FP recrossing in 14.5% of the fields in the PlexinA-DN condition but never in the controls (**Supplementary Fig. 2a**,**b**). In transverse sections, commissural axons abnormally entered the gray matter in 41% of the sections in the PlexinA-DN condition compared to only 5% in the controls (number of sections/number of embryos: 103/7 for embryos electroporated with GFP and empty vector; and 110/8 for embryos electroporated with GFP and PlexinA-DN) (**Supplementary Fig. 2c**,**d**). Notably, these phenotypes resembled those described in *Robo–Slit* mouse knockouts[12,17,19], suggesting that PlexinA1 could be the missing Slit commissural receptor.

Analysis of genetic interactions between Plxna1 and Robo-Slit

If PlexinA1, but not the Robos, mediates Slit midline barrier function, then PlexinA1 loss in the *Robo1*- and *Robo2*-null context should confer the midline recrossing phenotype observed in Slit mutants[17]. Other phenotypes present in *Robo1*-, *Robo2*- and *Plxna1*-null contexts should also be aggravated. We generated and analyzed a triple *Plxna1*, *Robo1* and *Robo2* mouse line. In open-book preparations of E12.5 embryos lacking either *Robo1* and *Robo2* ($n = 28$ crystals/3 embryos) or *Plxna1* ($n = 134$ crystals/13 embryos), we observed FP stalling in 41% and 47% of crystals, respectively, compared to only 19% in WT embryos ($n = 101$ crystals/10 embryos) and 22% in heterozygous

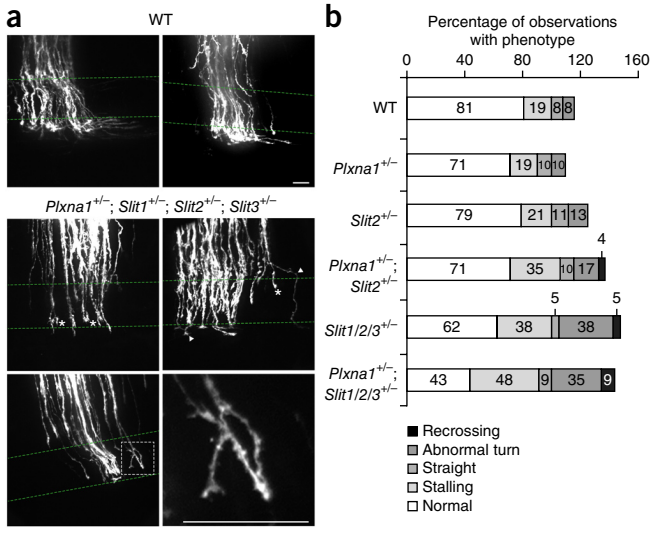

Figure 2 *PlexinA1* and *Slit* transheterozygotes exhibit a midline recrossing phenotype. (**a**) Microphotographs of DiI-labeled commissural tracts in WT embryos and misrouting phenotypes in *Plxna1*, *Slit1*, *Slit2* and *Slit3* quadruple heterozygous (*Plxna1*$^{+/-}$; *Slit1*$^{+/-}$; *Slit2*$^{+/-}$; *Slit3*$^{+/-}$) embryos with stalling (*), abnormal turning (arrowheads) and recrossing (dashed square). Scale bars, 25 µm. (**b**) Quantitative analysis of WT (n = 2 embryos, 26 crystals), *PlexinA1* heterozygous (*Plxna1*$^{+/-}$; n = 3 embryos, 31 crystals), *Slit2* heterozygous (*Slit2*$^{+/-}$; n = 4 embryos, 52 crystals), *PlexinA1* and *Slit2* double heterozygous (*Plxna1*$^{+/-}$; *Slit2*$^{+/-}$; n = 4 embryos, 57 crystals), *Slit1*, *Slit2* and *Slit3* triple heterozygous (*Slit1/2/3*$^{+/-}$; n = 2 embryos, 21 crystals) and *PlexinA1*, *Slit1*, *Slit2* and *Slit3* quadruple heterozygous (*Plxna1*$^{+/-}$; *Slit1/2/3*$^{+/-}$; n = 2 embryos, 23 crystals) embryos. Percentages of DiI crystals with each phenotype are indicated on the graph for each class of phenotype.

littermates (heterozygous for all three genes; n = 58 crystals/5 embryos) (**Fig. 1c**,**d**). However, in embryos lacking *Robo1*, *Robo2* and *Plxna1* (n = 36 crystals/3 embryos), FP stalling was increased to 78%, reaching the level described in *Slit1*, *Slit2* and *Slit3* triple mutants (**Fig. 1c**,**d**)[12]. Similarly, abnormal turning was increased to 72% in *Robo1*$^{-/-}$; *Robo2*$^{-/-}$; *Plxna1*$^{-/-}$embryos as compared to WT(6%), *Robo1*$^{-/-}$; *Robo2*$^{-/-}$ (26%) and *Plxna1*$^{-/-}$ (33%) embryos. We observed little FP recrossing in *Robo1*$^{-/-}$; *Robo2*$^{-/-}$ embryos, whereas FP recrossing reached the proportion reported for total Slit loss[12] in *Plxna1*$^{-/-}$ and in *Robo1*$^{-/-}$; *Robo2*$^{-/-}$; *Plxna1*$^{-/-}$ embryos (**Fig. 1c**,**d**).

We then generated Slit and PlexinA1 transheterozygotes to further genetically assess the interaction between PlexinA1 and Slits *in vivo* (**Fig. 2a**,**b**). Notably, we observed the recrossing phenotype in *Slit2*$^{+/-}$; *Plxna1*$^{+/-}$ embryos (4%, n = 57 crystals/4 embryos) but not in single *Plxna1*$^{+/-}$ (n = 31 crystals/3 embryos) or *Slit2*$^{+/-}$ embryos (n = 52 crystals/4 embryos). Moreover, loss of a single copy of *Plxna1* in *Slit1*$^{+/-}$; *Slit2*$^{+/-}$; *Slit3*$^{+/-}$ embryos (n = 23 crystals/2 embryos) increased the recrossing phenotype from 5% to 9% compared with *Plxna1*$^{+/+}$; *Slit1*$^{+/-}$; *Slit2*$^{+/-}$; *Slit3*$^{+/-}$ embryos (n = 21 crystals/2 embryos) (**Fig. 2a**,**b**).

Characterization of PlexinA1–Slit complexes

We next tested whether PlexinA1 and Slit family members could interact. We performed coimmunoprecipitations in COS7 cells using antibodies to pull down PlexinA1, Slit1 or Slit2. In all cases, Slit1 and Slit2 co-precipitated with PlexinA1 (**Fig. 3a** and **Supplementary Fig. 3a**). We also found that Slit1 coimmunoprecipitated with the PlexinA1 extracellular domain but not with PlexinA1 carrying a truncated intracellular and transmembrane domain or PlexinA1 lacking the intracellular domain and the four immunoglobulin-like, Plexin and transcription factor (IPT) domains (**Fig. 3b**,**c** and **Supplementary Fig. 3b**),

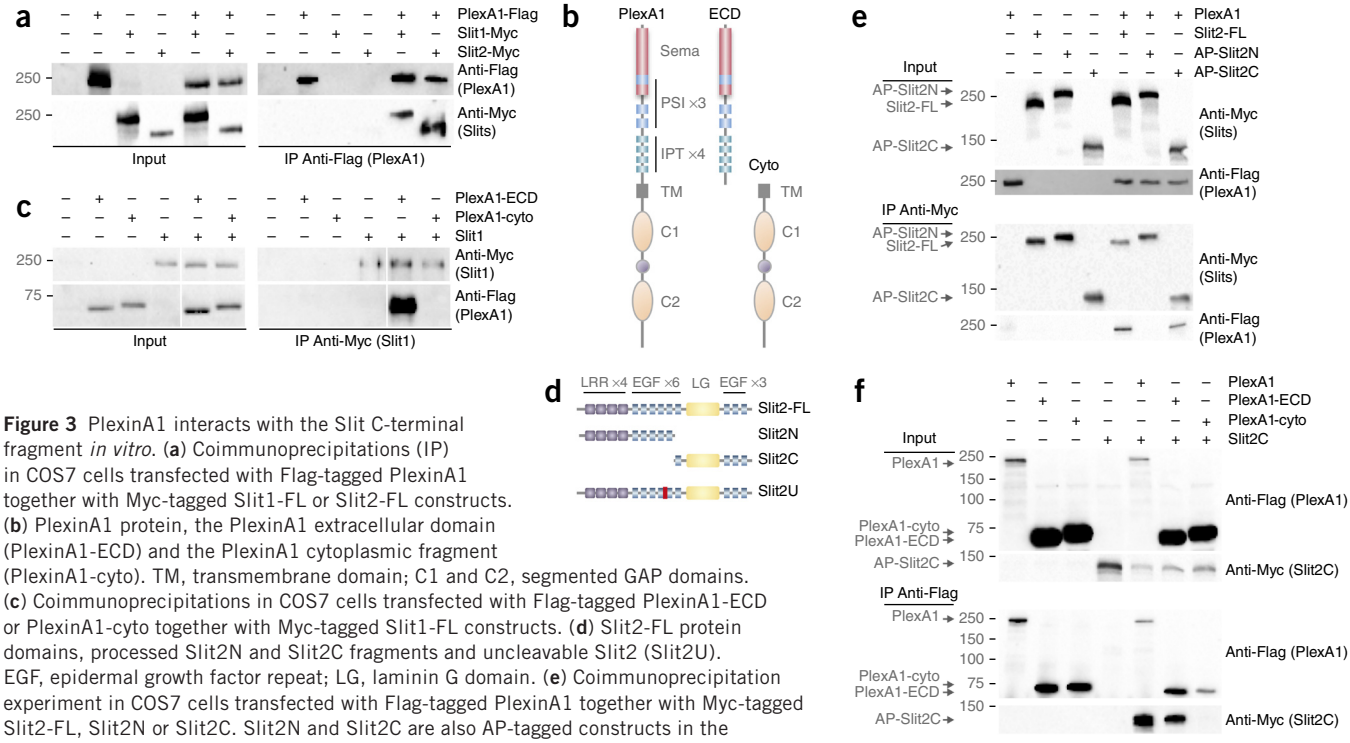

Figure 3 PlexinA1 interacts with the Slit C-terminal fragment *in vitro*. (**a**) Coimmunoprecipitations (IP) in COS7 cells transfected with Flag-tagged PlexinA1 together with Myc-tagged Slit1-FL or Slit2-FL constructs. (**b**) PlexinA1 protein, the PlexinA1 extracellular domain (PlexinA1-ECD) and the PlexinA1 cytoplasmic fragment (PlexinA1-cyto). TM, transmembrane domain; C1 and C2, segmented GAP domains. (**c**) Coimmunoprecipitations in COS7 cells transfected with Flag-tagged PlexinA1-ECD or PlexinA1-cyto together with Myc-tagged Slit1-FL constructs. (**d**) Slit2-FL protein domains, processed Slit2N and Slit2C fragments and uncleavable Slit2 (Slit2U). EGF, epidermal growth factor repeat; LG, laminin G domain. (**e**) Coimmunoprecipitation experiment in COS7 cells transfected with Flag-tagged PlexinA1 together with Myc-tagged Slit2-FL, Slit2N or Slit2C. Slit2N and Slit2C are also AP-tagged constructs in the N terminus. (**f**) Coimmunoprecipitations in COS7 cells transfected with Flag-tagged PlexinA1, PlexinA1-ECD or PlexinA1-cyto together with the Myc-tagged Slit2C construct. Full-length blots are presented in **Supplementary Figure 8**.

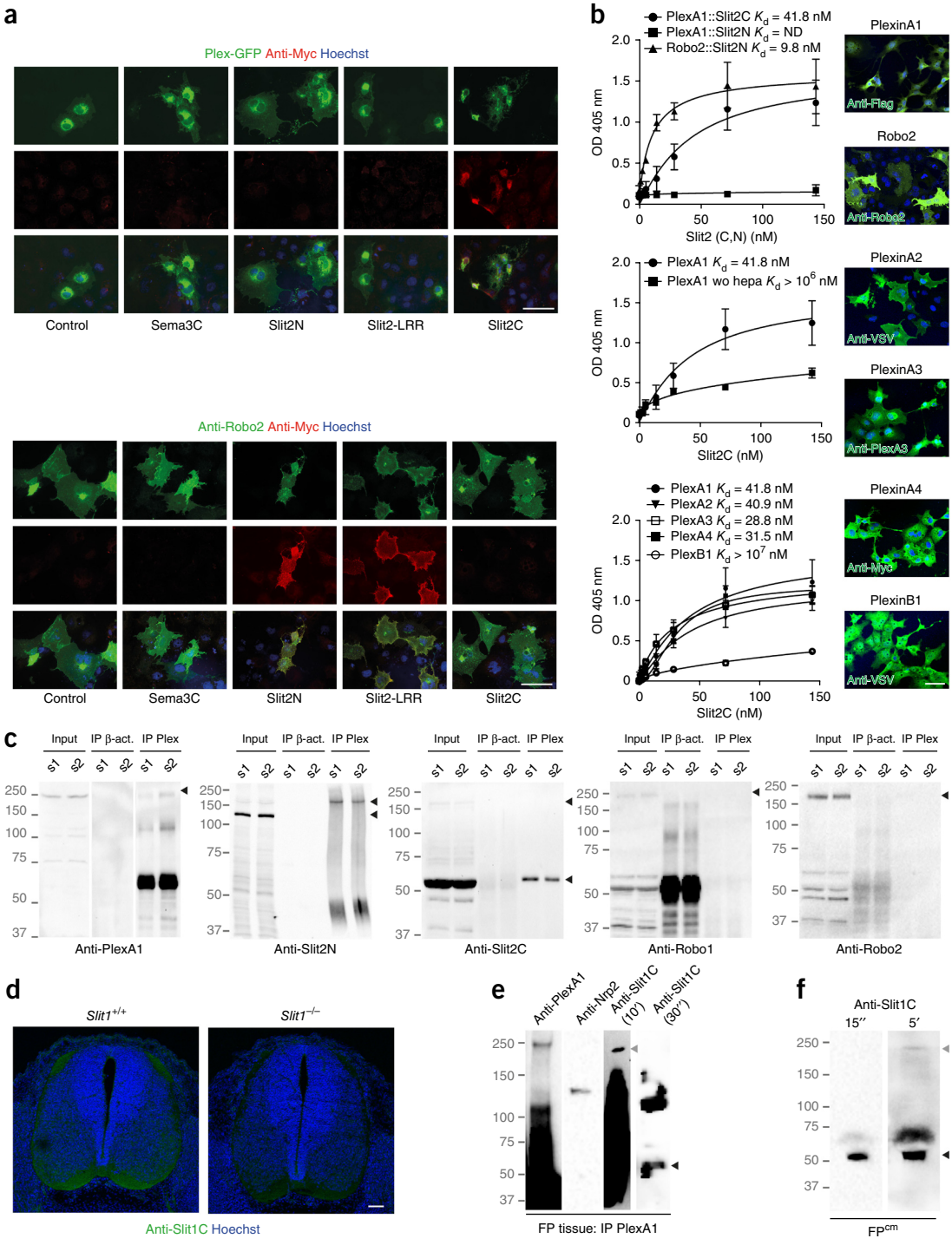

Figure 4 Slits bind PlexinA family members. (**a**) Binding experiments on COS7 cells transfected with GFP-tagged PlexinA1 (Plex-GFP, top) or Robo2 (bottom) and incubated with Myc-tagged Sema3C, Slit2N, Slit2-LRR or Slit2C. Binding was detected with Myc antibody. Scale bars, 50 µm. (**b**) Binding experiments in lysates of COS7 cells transfected with PlexinA1-Flag, Robo1, PlexinA2-VSV (vesicular stomatitis virus tag), PlexinA3, PlexinA4-Myc or PlexinB1-VSV and incubated with increasing concentrations of AP-tagged Slit2C or Slit2N. Binding was quantified by measuring AP activity. Right, immunofluorescent labeling of each transfected receptor in COS7 cells before lysis (scale bars, 50 µm). Binding curves were fitted using the Hill equation. K_d values were calculated according to the Hill equation. Error bars indicate the s.d. ND, not determined. OD 450 nm, optical density at 450 nm; wo hepa, without heparin. (**c**) Coimmunoprecipitation in E12.5 spinal cord lysates using PlexinA1 antibody and immunodetection of PlexinA1, Slit2 (using antibodies targeting an N-terminal or a C-terminal epitope), Robo1 and Robo2. s1 and s2 are two different samples, and arrowheads point to the predicted protein size. β-act., β-actin. (**d**) Immunofluorescent labeling of E12 spinal cord transverse sections using an antibody targeting a Slit1C epitope. Antibody specificity was assessed using sections from *Slit1*$^{+/+}$ and *Slit1*$^{-/-}$ embryos. Scale bar, 100 µm. (**e**) Coimmunoprecipitation of FP tissue lysates from E12.5 embryos using PlexinA1 antibody. Immunodetection of PlexinA1, Nrp2 and Slit1 (using antibody directed against a C-terminal epitope) is shown. ′ denotes minutes and ″ denotes seconds in **e** and **f**. (**f**) Immunodetection of Slit1 in medium conditioned by FP tissue using an antibody targeting a C-terminal epitope. In **e** and **f**, two exposures of the Slit1C immunoblot are shown to detect both the full-length protein (gray arrowhead) and the C-terminal cleavage fragment (black arrowhead).

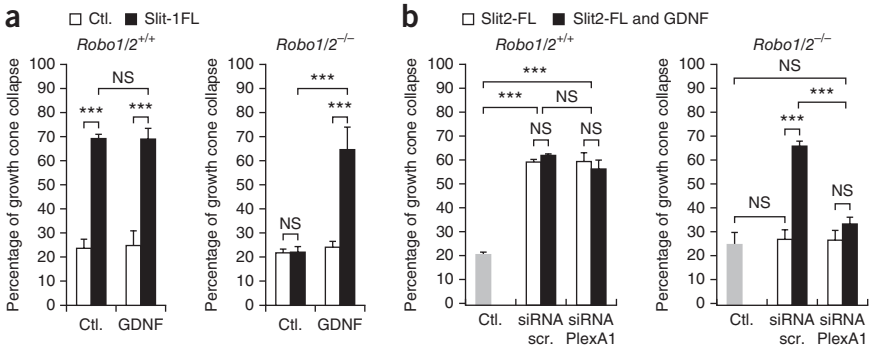

Figure 5 PlexinA1 is a functional receptor for Slits in commissural neurons. (**a**,**b**) Collapse assay on E12.5 *Robo1* and *Robo2* WT (*Robo1/2*$^{+/+}$) and null (*Robo1/2*$^{-/-}$) embryos incubated with Slit1-FL supernatant (**a**) or Slit2-FL supernatant (**b**) alone or together with GDNF. Ctl., control. In **b**, cells were transfected with either scrambled siRNA (siRNA scr.) or PlexinA1 siRNA. For **a** and **b**, $n = 4$ and $n = 6$ experiments per condition, respectively; the number of analyzed growth cones per condition was >200; and the graphs show the mean collapse rate ± s.d. ***$P < 0.001$, Student's t test. NS, not significant. In **a**, for *Robo1/2*$^{+/+}$, Ctl./Ctl. compared to Ctl./Slit1-FL: $P = 0.954$; for *Robo1/2*$^{-/-}$, Ctl./Slit1-FL compared to GDNF/Slit1-FL: $P = 0.872$. In **b**, for *Robo1/2*$^{+/+}$, siRNA scr./Slit2-FL compared to siRNA scr./Slit2-FL/GDNF: $P = 0.382$, siRNA PlexA1/Slit2-FL compared to siRNA PlexA1/Slit2-FL/GDNF: $P = 0.192$, siRNA scr./Slit2-FL compared to siRNA PlexA1/Slit2-FL/GDNF: $P = 0.156$; for *Robo1/2*$^{-/-}$, Ctl. compared to siRNA scr./Slit2-FL: $P = 0.422$, Ctl. compared to siRNA PlexA1/Slit2-FL: $P = 0.556$, siRNA PlexA1/Slit2-FL compared to siRNA PlexA1/Slit2-FL/GDNF: $P = 0.119$.

thus indicating that complex formation involves the Semaphorin (Sema)–Plexin, Semaphorin and integrin (PSI) extracellular domain of PlexinA1.

We then investigated which Slit2 N-terminal (Slit2N) and C-terminal (Slit2C) domain interacts with the PlexinA1 extracellular domain (**Fig. 3d**,**e**). We performed co-precipitation experiments with COS7 cells transfected with vectors encoding PlexinA1, Slit2-FL, Slit2N or Slit2C fragments. Both the Slit2-FL and Slit2C fragments coimmunoprecipitated with PlexinA1, but the Slit2N fragment did not (**Fig. 3e**). Thus, PlexinA1 interacts specifically with the C-terminal part of Slit (SlitC) that is complementary to the Robos, which bind SlitN[15]. Moreover, additional experiments confirmed that Slit2C co-precipitated with the PlexA1 extracellular domain but not with the intracellular domain (**Fig. 3f**).

We next assessed the PlexinA1-Slit interaction in *trans* in binding assays. We incubated COS7 cells transfected with PlexinA1 or Robo2 (as a positive control) in conditioned medium from HEK293T cells overexpressing Myc-tagged Slit2N, Slit2 leucine-rich region 2 (Slit2-LRR2, or Slit2-D2) or Slit2C (**Fig. 4a**). We detected bound proteins using Myc-specific antibody. As expected, Robo2-expressing cells bound both Slit2N and Slit2-LRR2 but not Slit2C (**Fig. 4a**). Conversely, PlexinA1-expressing cells bound Slit2C but neither Slit2N nor Slit2-LRR2. We then performed binding assays with alkaline phosphatase (AP)-tagged Slits to measure the affinity of PlexinA1-Slit2C binding. We calculated a K_d of 41.8 nM for PlexinA1-Slit2C, whereas we found a K_d of 9.8 nM for Robo2-Slit2N, consistent with a previous report[15] (**Fig. 4b**). Robo-Slit binding affinity has been reported to depend on heparan sulfate proteoglycans. Similarly, we found that heparin removal markedly lowered Slit2C-PlexinA1 binding affinity (**Fig. 4b**). We also examined whether PlexinA1 shares binding to SlitC with other Plexins. We found that all PlexinAs (PlexinA1, PlexinA2, PlexinA3 and PlexinA4) interacted with Slit2C with comparable affinities, whereas PlexinB1 showed no binding to Slit2C (**Fig. 4b**).

Next, to determine whether Slit–PlexinA1 complexes form *in vivo*, we performed coimmunoprecipitation experiments on E12.5 mouse spinal cord lysates. Using an antibody directed against the Slit2 C-terminal fragment, we detected Slit2C in the PlexinA1-immunoprecipitated fraction (**Fig. 4c**). Reciprocally, endogenous PlexinA1 was present in the Slit2C-immunoprecipitated fraction, confirming that the complex exists *in vivo* (**Supplementary Fig. 3c**). Using an antibody directed against an epitope in the Slit2 N-terminal region, we detected co-precipitation of PlexinA1 with Slit2-FL but not Slit2N. We did not detect either Robo1 or Robo2 in these complexes, thus confirming that the PlexinA1-Slit2C interaction does not require Robo receptors (**Fig. 4c**). Slit1-FL also co-precipitated with PlexinA1. Slit1C migrated close to crossreacting immunoglobulins in western blot analysis but could still be distinguished (**Supplementary Fig. 3d**). We detected the PlexinA1–Slit1 complex in spinal cord extracts from both *Robo1*$^{+/+}$; *Robo2*$^{+/+}$ and *Robo1*$^{-/-}$; *Robo2*$^{-/-}$ embryos, also confirming that Robos are dispensable for PlexinA1–Slit complex formation (**Supplementary Fig. 3d**).

These data further support that PlexinA1 might act as a Slit receptor *in vivo*, mediating Slit-FL and SlitC functions during commissural axon guidance. Immunohistochemical labeling of E12 spinal cords using antibody to a Slit1 C-terminal epitope showed that the protein is detected, as would be expected from its RNA pattern, in the FP and motoneuron domain (**Fig. 4d**). We could not assess the distribution of the Slit fragments, as available antibodies collectively recognize the full-length protein and the corresponding processed fragment containing the target epitope. To confirm the presence of the Slit–PlexinA1 complex during midline crossing, we dissected out FP tissue from E12.5 embryos and precipitated it with PlexinA1. As expected, Neuropilin2 (Nrp2) co-precipitated with PlexinA1, as well as with Slit1-FL and Slit1C (**Fig. 4e**). Moreover, we detected the Slit1C fragment in medium conditioned with isolated FPs (**Fig. 4f**). Overall, these observations support that SlitC fragments are present in the FP by the time commissural axons navigate at the midline.

PlexinA1 mediates Slit commissural growth cone collapse

Next we studied whether PlexinA1 could act as a functional receptor for Slit family members in commissural neurons independently of Robo receptors. To dissociate the contributions of Robo and PlexinA1, we took advantage of our previous finding that PlexinA1 growth cone surface expression is prevented in dissociated commissural neuron cultures because of calpain-mediated processing, unless cells are exposed to glial cell line–derived neurotrophic factor (GDNF)[7,8] (**Supplementary Fig. 4**). Thus, exposing *Robo1*$^{-/-}$; *Robo2*$^{-/-}$ commissural neurons to GDNF or FP conditioned medium or leaving them unexposed allowed us to assess PlexinA1 activity specifically (**Supplementary Fig. 4**).

We treated cultured neurons isolated from E12.5 *Robo1*$^{+/+}$; *Robo2*$^{+/+}$ and *Robo1*$^{-/-}$; *Robo2*$^{-/-}$ embryos with Slit1-FL supernatant. In the absence of GDNF, Slit1-FL induced significant growth cone collapse in WT but not *Robo1*$^{-/-}$; *Robo2*$^{-/-}$ neurons (**Fig. 5a**). Notably, combined treatment with Slit1-FL and GDNF—inducing PlexinA1 surface expression—triggered significant collapse of *Robo1*$^{-/-}$; *Robo2*$^{-/-}$

commissural growth cones (**Fig. 5a**). Similarly, Slit2-FL elicited a significant growth cone collapse response in GDNF-treated commissural neurons (**Fig. 5b**). Transfection of *PlexinA1* siRNA but not scrambled siRNA in *Robo1*$^{-/-}$; *Robo2*$^{-/-}$ commissural neurons was sufficient to suppress this response (**Fig. 5b** and **Supplementary Fig. 5a**). This observation revealed a PlexinA1-dependent, Robo1- and Robo2-independent Slit-induced commissural responsiveness.

SlitC is a repulsive cue for PlexinA1^{+} commissural axons

Our results raised the intriguing possibility that SlitC fragments could have biological activity through PlexinA1. We first used collapse assays to compare the properties of Slit supernatants in E12.5 cultured commissural neurons, either treated or not with FP conditioned medium (FP^{cm}), triggering PlexinA1 cell surface expression. We controlled the presence of the different Slit forms in the supernatants by western blotting (**Fig. 6a**). The Slit1-FL, Slit2-FL and Slit2N supernatants elicited significant increases in the rate of growth cone collapse in the absence of FP^{cm} (**Fig. 6b**). In contrast, Slit2C had no such basal effect but could collapse FP^{cm}-treated commissural growth cones (**Fig. 6b**). Transfection of *PlexinA1* siRNA but not scrambled siRNA drastically reduced Slit2C collapse activity and the response to Sema3B, used as a positive control (**Fig. 6c**). Moreover *Robo1*$^{-/-}$;

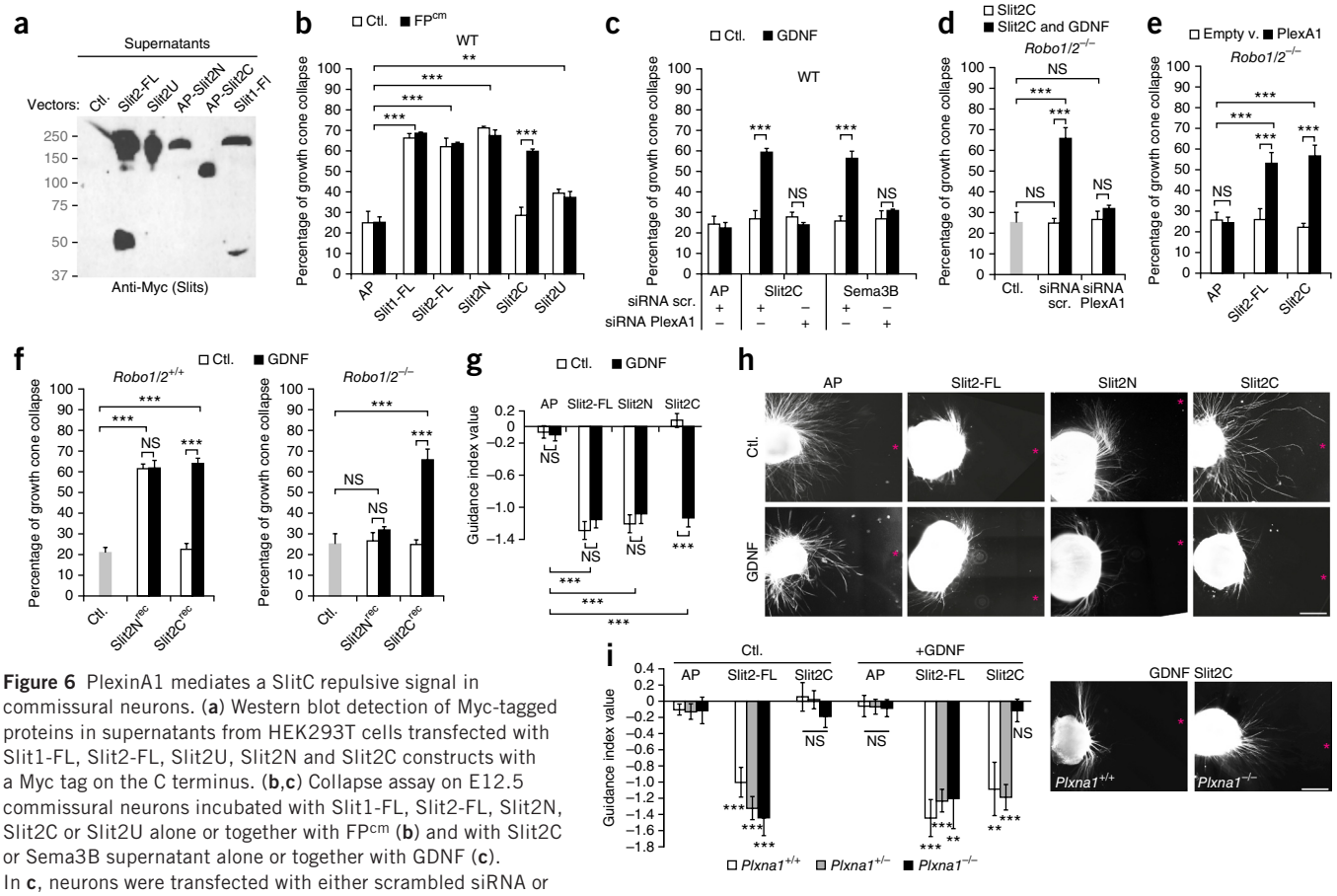

Figure 6 PlexinA1 mediates a SlitC repulsive signal in commissural neurons. (**a**) Western blot detection of Myc-tagged proteins in supernatants from HEK293T cells transfected with Slit1-FL, Slit2-FL, Slit2U, Slit2N and Slit2C constructs with a Myc tag on the C terminus. (**b**,**c**) Collapse assay on E12.5 commissural neurons incubated with Slit1-FL, Slit2-FL, Slit2N, Slit2C or Slit2U alone or together with FP^{cm} (**b**) and with Slit2C or Sema3B supernatant alone or together with GDNF (**c**). In **c**, neurons were transfected with either scrambled siRNA or PlexA1 siRNA. (**d**) Collapse assay performed on commissural neurons from E12.5 *Robo1/2*$^{-/-}$ embryos incubated with Slit2C supernatant alone or together with GDNF and transfected either with scrambled siRNA or PlexA1 siRNA. (**e**) Collapse assay performed on commissural neurons from E12.5 *Robo1/2*$^{-/-}$ embryos transfected with a PlexinA1 construct and incubated with Slit2-FL or Slit2C supernatants. Empty v., empty vector. (**f**) Collapse assay performed on commissural neurons from E12.5 WT and *Robo1/2*$^{-/-}$ embryos transfected with a PlexinA1 construct and incubated with 2 mg/l recombinant Slit2C (Slit2C^{rec}) or Slit2N (Slit2N^{rec}). For **b**, **c**, **e** and **f**, $n = 4$ experiments; the number of analyzed growth cones per condition was >100. For **d**, $n = 6$ experiments; the number of analyzed growth cones per condition was >150. For **b**–**f**, graphs show the mean collapse rate ± s.d. $^{*}P < 0.05$, $^{**}P < 0.01$, $^{***}P < 0.001$, Student's *t* test. NS, not significant. In **b**, AP/Ctl. compared to Slit2U/Ctl.: $P = 0.012$. In **c**, Slit2C/Ctl./siRNA PlexA1 compared to Slit2C/GDNF/siRNA PlexA1: $P = 0.038$, Sema3B/Ctl./siRNA PlexA1 compared to Sema3B/GDNF/siRNA PlexA1: $P = 0.106$. In **d**, Ctl. compared to siRNA scr./Slit2C: $P = 0.834$, siRNA PlexA1/Slit2C compared to siRNA PlexA1/Slit2C/GDNF: $P = 0.198$, Ctl. compared to siRNA PlexA1/Slit2C: $P = 0.901$. In **e**, AP/Ctl. compared to AP/PlexA1: $P = 0.880$. In **f**, for *Robo1/2*$^{+/+}$, Slit2N^{rec}/Ctl. compared to Slit2N^{rec}/GDNF: $P = 0.882$; for *Robo1/2*$^{-/-}$, Ctl. compared to Slit2N^{rec}/Ctl.: P=0.642, Slit2N^{rec}/Ctl. compared to Slit2N^{rec}/GDNF: $P = 0.072$. (**g**,**h**) Microphotographs (**g**) and quantification (**h**) of dorsal spinal cord explants cultured with HEK293T cell aggregates expressing Slit2-FL, Slit2N or Slit2C alone or together with GDNF. Red stars indicate aggregate positions. Axon trajectories were scored blindly with a guidance index ranging from –2 to +2 (the number of explants per condition was >40). Scale bar, 100 µm. (**i**) Quantification of cocultures of dorsal spinal cord explants from *Plxna1* WT, heterozygous and null embryos (the number of explants per condition was >6) Scale bar, 100 µm. For **g** and **i**, the graph shows the mean index ± s.e.m. $^{**}P < 0.01$, $^{***}P < 0.001$, Mann-Whitney *U* test. In **g**, AP/Ctl. compared to AP/GDNF: $P = 0.808$, Slit2-FL/Ctl. compared to Slit2-FL/GDNF: $P = 0.465$, Slit2N/Ctl. compared to Slit2N/GDNF: $P = 0.548$. In **i**, in the Ctl. condition, Slit2C *Plxna1*$^{+/+}$ compared to *Plxna1*$^{+/-}$: $P = 0.840$, Slit2C *Plxna1*$^{+/+}$ compared to *Plxna1*$^{-/-}$: $P = 0.362$; in the GDNF condition, AP *Plxna1*$^{+/+}$ compared to *Plxna1*$^{+/-}$: $P = 0.967$, AP *Plxna1*$^{+/+}$ compared to *Plxna1*$^{-/-}$: $P = 0.887$, AP *Plxna1*$^{-/-}$ compared to Slit2C *Plxna1*$^{-/-}$: $P = 0.943$, AP *Plxna1*$^{-/-}$ compared to Slit2FL *Plxna1*$^{-/-}$: $P = 0.0078$, AP *Plxna1*$^{+/+}$ compared to Slit2C *Plxna1*$^{+/+}$: $P = 0.0063$.

Robo2$^{-/-}$ commissural growth cones exposed to GDNF and Slit2-FL or GDNF and Slit2C could still be collapsed, whereas neither Slit2-FL nor Slit2C alone induced such a response (**Figs. 5b** and **6d**). Growth cone collapse in response to Slit2-FL or Slit2C was abolished in commissural neurons transfected with *PlexinA1* siRNA (**Figs. 5b** and **6d**). Likewise, the collapse activity of GDNF and Slit2C was lost in *Plxna1*-null commissural growth cones (**Supplementary Fig. 5b**). We have shown previously that PlexinA1 overexpression in commissural neurons overcomes the endogenous GDNF-dependent regulation of PlexinA1 and significantly increases the level of PlexinA1 expression at the growth cone surface[7]. Indeed, *Robo1*$^{-/-}$; *Robo2*$^{-/-}$ commissural growth cones overexpressing PlexinA1 were collapsed by

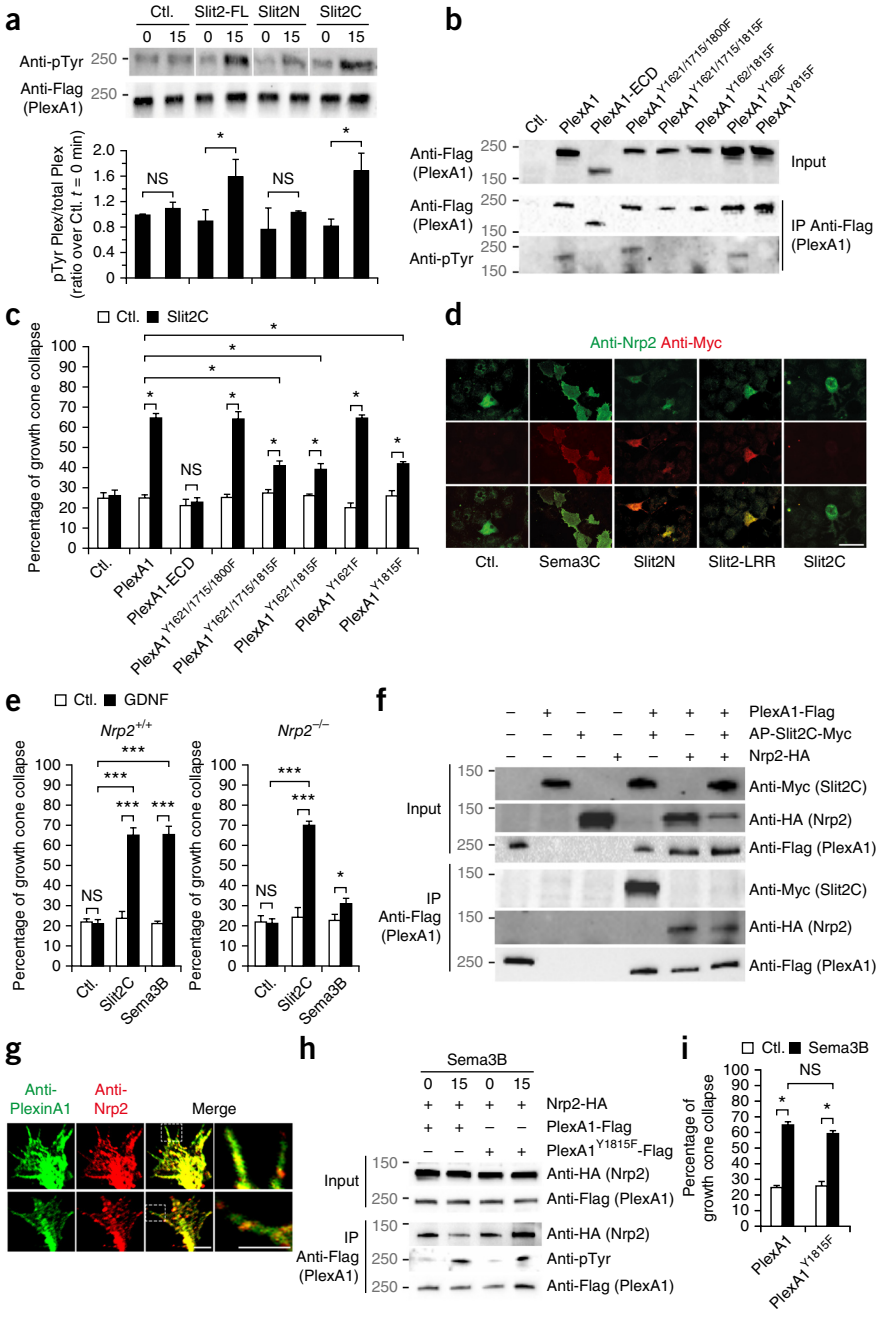

Figure 7 Slits and Semaphorins mediate specific PlexinA1 activation. (**a**) Immunoprecipitation experiment performed on Flag-tagged PlexinA1-expressing COS7 cells incubated with Slit2-FL, Slit2N or Slit2C supernatants for 15 min. Phosphorylated PlexinA1 is detected within PlexinA1 immunoprecipitates using antibody to phosphorylated tyrosine (anti-pTyr) (top). The graph on the bottom shows quantification of the ratio of phosphorylated PlexinA1 to total PlexinA1. **P* = 0.049, Ctl. 0 min compared to 15 min: *P* = 0.513, Slit2N 0 min compared to 15 min: *P* = 0.275, Mann-Whitney *U* test. NS, not significant. (**b**) Immunoprecipitation in COS7 cells transfected with Flag-tagged PlexinA1, PlexinA1-ECD or PlexinA1 tyrosine triple, double or single mutants and incubated with Slit2C supernatant for 15 min. Phosphorylated PlexinA1 is detected within anti-Flag immunoprecipitates using antibodies to pTyr. (**c**) Collapse assay performed on commissural neurons from E12.5 embryos transfected with PlexinA1, PlexinA1-ECD or PlexinA1 tyrosine triple, double or single mutants and incubated with Slit2C supernatant. *n* = 3 experiments per condition; the number of analyzed growth cones per condition was >100; and the graph shows the mean collapse rate ± s.d. **P* = 0.049, PlexA1-ECD Ctl. compared to Slit2C: *P* = 0.4, Mann-Whitney *U* test. NS, not significant. (**d**) Binding experiments performed on COS7 cells transfected with a Nrp2 construct and incubated with supernatants from cells expressing Myc-tagged Sema3C, Slit2N, Slit2-LRR or Slit2C. Binding was detected using a Myc antibody. Scale bar, 50 µm. (**e**) Collapse assay performed on commissural neurons from E12.5 WT and *Nrp2*-null embryos incubated with Slit2C or Sema3B supernatant alone or together with GDNF. *n* = 4 experiments per condition; the number of analyzed growth cones per condition was >200; and graphs show the mean collapse rate ± s.d. **P* < 0.05, ****P* < 0.001, Student's *t* test. NS, not significant. For *Nrp2*$^{+/+}$, Ctl./Ctl. compared to Ctl./GDNF: *P* = 0.608. For *Nrp2*$^{-/-}$, Ctl./Ctl. compared to Ctl./GDNF: *P* = 0.822, Sema3B/Ctl. Compared to Sema3B/GDNF: *P* = 0.033. (**f**) Coimmunoprecipitation experiment in COS7 cells transfected with Flag-tagged PlexinA1 together with Myc-tagged Slit2C and/or HA-tagged Nrp2. The Slit2C construct is also tagged with AP at the N terminus. (**g**) Immunofluorescent labeling of endogenous PlexinA1 and Nrp2 in WT commissural growth cones previously treated with GDNF using PlexinA1 and Nrp2 antibodies. Scale bars, 10 µm. The images on the far right are enlargements of the boxed areas in the images to the left. (**h**) Immunoprecipitation experiment in COS7 cells transfected with an HA-tagged Nrp2 construct together with Flag-tagged PlexinA1 or the PlexinA1^{Y1815F} mutant and incubated with Sema3B supernatant for 15 min. Phosphorylated PlexinA1 is detected within anti-Flag immunoprecipitates using antibody to pTyr. (**i**) Collapse assay performed on commissural neurons from E12.5 embryos transfected with PlexinA1 or the PlexinA1^{Y1815F} mutant and incubated with Sema3B supernatant. *n* = 3 experiments per condition; the number of analyzed growth cones per condition was >100. **P* = 0.049, PlexinA1/GDNF compared to PlexinA1^{Y1815F}/GDNF: *P* = 0.127, Mann-Whitney *U* test. NS, not significant. Full-length blots are presented in **Supplementary Figure 9**.

Slit2-FL and Slit2C (**Fig. 6e**). These assays revealed that Slit2C has collapsing activity. Slit1C was also able to induce the collapse of GDNF-treated commissural growth cones (**Supplementary Fig. 5c**). To confirm that Slits in the supernatants were responsible for the effects observed, we performed collapse assays with recombinant Slit2C ($Slit2C^{rec}$) and Slit2N ($Slit2N^{rec}$) on WT and *Robo1*$^{-/-}$; *Robo2*$^{-/-}$ commissural neurons. As expected, in both WT and *Robo1*$^{-/-}$; *Robo2*$^{-/-}$ neurons, $Slit2C^{rec}$ elicited a robust collapse response in GDNF-treated commissural growth cones, whereas it had no effect in the basal condition (**Fig. 6f**). Conversely, the $Slit2N^{rec}$-induced collapse observed in WT neurons was lost in *Robo1*$^{-/-}$; *Robo2*$^{-/-}$ neurons independently of GDNF treatment (**Fig. 6f**).

Next we assessed whether Slit2C exerts PlexinA1-mediated repulsion. We cocultured dorsal spinal cord explants with HEK293T cell aggregates secreting Slit2-FL, Slit2N or Slit2C alone or in combination with GDNF. We examined axon trajectories and classified them as described in refs. 8 and 20 (**Fig. 6g**,**h**). Axon trajectories were oriented randomly in both control and GDNF-exposed explants, as described previously[8]. In contrast, axons were deflected away from cell aggregates secreting Slit2-FL and Slit2N alone and in combination with GDNF (**Fig. 6g**,**h**). Notably, although they were oriented randomly in the Slit2C condition, axons gained significant repulsion in the Slit2C and GDNF condition (**Fig. 6g**,**h**). This effect was lost in cocultures of *Plxna1*$^{-/-}$ explants (**Fig. 6i**). We then assessed whether SlitN-Robo and SlitC-PlexinA1 signaling could have a synergistic collapsing effect on commissural growth cones. We treated commissural growth cones with FP^{cm} or GDNF to induce PlexinA1 surface expression and exposed them to optimal and suboptimal doses of Slit2-FL supernatant. We observed that suboptimal doses of Slit2-FL induced a higher collapse rate in neurons primed with FP^{cm} or GDNF than in naive neurons and than when Slit2-FL was applied alone, thus suggesting that the two types of signaling can act in parallel (**Supplementary Fig. 5d**).

PlexinA1 mediates Slit signaling

Our data were all consistent with PlexinA1 being a functional Slit receptor. We thus investigated whether Slits can induce activation of the PlexinA1 receptor and downstream signaling. We first assessed early events of receptor activation and searched for tyrosine phosphorylation, as has been reported for PlexinA1 and PlexinB proteins downstream of Semaphorins[21–23].

We stimulated PlexinA1-expressing COS7 cells with supernatants from cells transfected with vectors encoding Slit2-FL, Slit2N or Slit2C, each fused with an Myc tag on the C terminus. After 15 min of exposure, we immunoprecipitated PlexinA1 and probed it with an antibody to phosphorylated tyrosine. Slit2-FL and Slit2C, but not Slit2N, significantly induced PlexinA1 phosphorylation (**Fig. 7a**). To identify the tyrosine(s) phosphorylated by Slit, we conducted a bioinformatics prediction with NetPhos 2.0 (ref. 24), which designated 5 tyrosines over the 22 tyrosines contained in the PlexinA1 intracellular domain. We generated single, double and triple tyrosine mutants using tyrosine-to-phenylalanine substitutions and assessed the receptor phosphorylation status after treatment with Slit2C. We observed that PlexinA1 harboring Y1621F, Y1715F and Y1800F ($PlexinA1^{Y1621/1715/1800F}$) and $PlexinA1^{Y1621F}$ retained full phosphorylation, whereas the phosphorylation of $PlexinA1^{Y1621/1715/1815F}$, $PlexinA1^{Y1621/1815F}$ and $PlexinA1^{Y1815F}$ was markedly reduced (**Fig. 7b**). Thus, Slit2C induces PlexinA1 phosphorylation on Y1815. Next, we overexpressed the PlexinA1 tyrosine mutants in commissural neurons and assessed their ability to mediate Slit collapse. Notably, mutations that did not interfere with Slit-induced PlexinA1 phosphorylation had no impact on the collapse response of commissural growth cones to Slit2C (**Fig. 7c**). In contrast, substitution of Y1815 in single, double and triple mutants significantly altered the collapse response (**Fig. 7c**). Thus, PlexinA1 Y1815 phosphorylation is necessary for growth cone collapse by SlitC. Next we examined activation of the Rho GTPase Rac1. Rac1 acts upstream and downstream of PlexinA1 to regulate PlexinA1 activity, and as such, the amount of Rac1-bound GTP is increased in the presence of active PlexinA1 (refs. 25,26). Regulation of Rac activity is also associated with axonal responses to various guidance cues, including Slits and Semaphorins[27–29]. We observed a significant (P = 0.049, Mann-Whitney U test) increase in active Rac1-GTP after treatment with Slit1-FL, Slit2-FL or Slit2C but not Slit2N, thus showing that PlexinA1-Slit can trigger Rac1 activation (**Supplementary Fig. 6a**). Similarly, we observed robust phosphorylation of the MAPK ERK1/2, which has been implicated in axon guidance signaling[30], in cells treated with Slit2-FL and Slit2C (**Supplementary Fig. 6b**). Thus, SlitC triggers specific PlexinA1 phosphorylation and downstream signaling that is known to regulate growth cone behaviors.

Slits and Semaphorins trigger specific PlexinA1 activation

Because PlexinA1 is recruited to Nrp2 to mediate the effect of Sema3B during commissural axon guidance[7], we wondered whether Nrp2 is a component of the Slit–PlexinA1 complex, whether it also binds Slits and whether Sema3B and Slit signaling share a common mechanism of PlexinA1 activation. In binding assays, we observed that Nrp2-expressing cells could bind Sema3C as a positive control and could bind weakly to Slit2N and Slit2-LRR2 but not Slit2C (**Fig. 7d**). In addition, we found that commissural neurons dissected from *Nrp2*$^{-/-}$ embryos were as competent as their *Nrp2*$^{+/+}$ counterparts to collapse in response to Slit2C, thus demonstrating that Nrp2 is dispensable for PlexinA1-Slit signaling (**Fig. 7e**).

Next we found that Slit co-precipitated with PlexinA1 in cells expressing PlexinA1 alone but not in cells coexpressing Nrp2 and PlexinA1 (**Fig. 7f**). This observation suggests that navigating commissural growth cones might have distinct PlexinA1 receptor pools, either associating or not with Nrp2. In support of this idea, immunohistochemical detection of Nrp2 and PlexinA1 in GDNF-treated commissural growth cones revealed that PlexinA1 and Nrp2 have only partially overlapping distributions (**Fig. 7g**). We then investigated whether PlexinA1 is similarly activated by Sema3B and Slit, and thus when it is associated or not associated with Nrp2. We examined whether Sema3B could induce PlexinA1 phosphorylation in cells expressing PlexinA1 and Nrp2 and, if so, whether this requires Y1815. Remarkably, we detected Sema3B-induced PlexinA1 phosphorylation, but the Y1815F mutation did not prevent it (**Fig. 7h**). Moreover, although it abolished the Slit-mediated collapse effect, overexpression of the $PlexinA1^{Y1815F}$ mutant in commissural neurons did not alter their Sema3B-induced collapse response (**Fig. 7i**).

DISCUSSION

Our study establishes that PlexinA1, a well-known Semaphorin receptor, is also a receptor for Slits. Our phenotypic analysis of various mouse models together with results from biochemical approaches and functional assays support this conclusion and define an *in vivo* contribution of Plexin-Slit signaling during commissural axon guidance. We also report for the first time, to our knowledge, bioactivity of the C-terminal fragment generated by Slit processing and show its requirement in commissural axon guidance.

PlexinA1 is a receptor for Slits

In the *Drosophila* ventral cord, loss of Robo-Slit signaling induces multiple recrossings, altering commissure formation[4,9,10]. Analysis of mutant mouse models established a conserved function of Robo-Slit signaling at the spinal cord midline[4,5,16]. In mice, simultaneous loss of all Slits (Slit1, Slit2 and Slit3) leads some growth cones to turn back and recross the midline[12]. However, embryos lacking both Robo1 and Robo2 only have a few recrossing axons and fewer stalling fibers, supporting the existence of another Slit receptor[17]. Analysis of brain commissures and olfactory projections in Robo and Slit mutants have also drawn similar conclusions[31,32].

Although we observed that *in vitro* SlitC can bind to all PlexinAs, our data strongly support that PlexinA1 is the Slit receptor in spinal commissures. Embryos lacking PlexinA1 but not Robo1 and Robo2 exhibited the recrossing phenotype typical of Slit1-, Slit2- and Slit3-deficient embryos. Abrogation of *Plxna1* in a *Robo1*; *Robo2* knockout background was sufficient to confer this recrossing phenotype. The analysis of *Plxna1*; *Slit1*; *Slit2*; *Slit3* transheterozygotes also suggested that PlexinA1 interacts with Slits. In addition, we did not detect recrossing in embryos lacking *Sema3B*, thus indicating that the underlying PlexinA1 function is independent of Sema3B. In binding assays and biochemical experiments, Slits could bind PlexinA1 and trigger its activation, and PlexinA1–Slit complexes could be detected in the developing spinal cord. *Ex vivo*, PlexinA1 could mediate a repulsive effect of Slits in spinal commissural axons independently of the Robos and Neuropilins. This specific contribution of PlexinA1 over other PlexinAs could be caused by structural features unique to PlexinA1 or, alternatively, to differences of PlexinA expression profiles in commissural neurons, as has been observed previously[7].

Selective contribution of Slit fragments and Sema3B

The phenotypic diversity of midline crossing defects in mutant mice indicates that midline repellents have specific functions during commissural axon navigation. Indeed, while Sema3B and Slit proteins are available in the FP to exert repulsive action, the recrossing phenotype is only seen in the context of Slit deficiency. Moreover, the cleavage of Slit-FL in the FP generates processed fragments, but the lack of a recrossing phenotype in the Robo mutants indicates that SlitN fragments are unlikely to have a major role in preventing midline recrossing. First, these distinct contributions might be set by functional specificities. Slit-FL and SlitN proteins could have distinct properties, even though both bind the Robos. For example, Slit2N, but not Slit2-FL, has been reported to collapse olfactory bulb axons[15,16]. Second, the diverse repellents are also probably differently distributed. The expression domains of Slit-FL proteins and their fragments are not well documented, as antibodies distinguishing each Slit protein form and fragment by immunohistochemistry are lacking. Expression patterns of Slit proteins might rely on their interactions with components of the extracellular matrix and the surrounding cell surfaces, such as heparan sulfate glycosaminoglycans. Accordingly, the spatial distribution of Slit proteins is modified in the *Drosophila* syndecan mutant[33]. Collagen IV binds Slit1 and distributes the protein at the surface of the tectum[34]. Third, Slit distribution profiles depend intimately on the unknown mechanisms controlling their proteolytic cleavage. The ratio of full-length to processed Slits might be tightly controlled and variable in different contexts. Indeed, we detected Slit processing more easily in HEK293T than COS7 cells (data not shown). Slit was recently shown to bind to dystroglycan deposited in the FP and at the basal membrane[35]. Because SlitC but not SlitN contains the dystroglycan-binding laminin G domain[35], the SlitC fragment might accumulate at the FP. Accordingly, we could detect Slit1C in conditioned medium from isolated FP cultures. The specific dynamics of Robo and PlexinA1 receptors in commissural growth cones are probably a crucial parameter, giving the tempo of the sensitization of commissural growth cones to midline repellents. PlexinA1 cell surface expression is induced in crossing and post-crossing tracts[7]. Although still poorly documented, control of Robo receptor expression during commissural growth cone sensitization to Slits is supported by recent data suggesting that regulated exocytosis switches Robo1 levels from low to high at the midline[36]. Thus, an interesting possibility would be that that the contribution of PlexinA1, but not Robos, in preventing midline recrossing relies on temporal differences in the availability of the receptors at the growth cone surface during FP navigation.

SlitC processed fragments have biological activity

We show here that the SlitC fragment is not inactive as initially thought (based on its inability to bind Robo[16]), but rather that it acts through PlexinA1 as a chemorepellent. SlitC activity is conditioned by the availability of PlexinA1 at the growth cone surface, which is controlled through regulated proteolytic processing. Hence, SlitC had no effect on naive commissural neurons and explants. In contrast, SlitC-induced repulsion was switched on when we primed commissural neurons with FP^{cm} or GDNF, which suppresses PlexinA1 processing and restores PlexinA1 levels[7,8]. Because PlexinA1 growth cone expression is switched on at the midline, SlitC might act as a crossing and post-crossing chemorepellent, preventing midline recrossing. Our finding that the SlitC fragment is bioactive provides alternative interpretation of previous studies that reported different effects of Slit-FL (containing both processed fragments) and SlitN supernatants, for example, on cortical neurons[37].

Midline repellents activate shared and specific receptors

We found that PlexinA1 is a receptor shared by Semaphorins and Slits. This probably applies to all PlexinA family members, as we observed that they all bind Slits, but probably not to other Plexins, as PlexinB1 did not bind Slit. These findings open a potential contribution of PlexinA-Slit signaling in broader contexts, particularly in tumorigenesis and immunity, where Plexins and Slits have prominent roles[38,39].

Our study reveals specific mechanism of PlexinA1 activation by Slit and Sema3B. Remarkably, although both ligands induce PlexinA1 phosphorylation, the phosphorylation sites differ, as we found that Y1815 is phosphorylated by Slit but not by Sema3B. This phosphorylation might be required for signal transduction or, alternatively, for triggering specific receptor trafficking or subunit assembly. Moreover, PlexinA1-Slit binding is prevented when PlexinA1 is recruited to Nrp2, indicating that PlexinA1 participates in distinct signaling. Both free and Nrp2-bound PlexinA1 pools exist in commissural growth cones, which may allow for parallel processing of Slit and Sema3B signaling. This idea is consistent with previous results on EphA and EphrinA coexpression in motoneuron growth cones that triggers parallel forward and reverse Eph-Ephrin signaling[40]. Thus, during their navigation across the midline, commissural growth cones might assemble various types of receptors in time and space to mediate the selective contributions of the diverse midline repellents (**Supplementary Fig. 7**).

METHODS

Methods and any associated references are available in the online version of the paper.

Note: Any Supplementary Information and Source Data files are available in the online version of the paper.

ACKNOWLEDGMENTS

V.C. is supported by grants from the French National Research Agency (ANR-2010-BLANC-1430-01) and the European Research Council under the European Union's Seventh Framework Programme (FP/2007-2013)/ERC Grant Agreement 281604-YODA. C.D.-B. is supported by a post-doc fellowship from the 'Ligue Contre le cancer'. This work was performed within the framework of the LABEX CORTEX and the LABEX DevWeCan of Université de Lyon within the program 'Investissements d'Avenir' (ANR-11-IDEX-0007) operated by the French National Research Agency (ANR). A.C. is supported by grants from the Fondation pour la Recherche Médicale (Programme 'équipe FRM') and the Agence Nationale de la Recherche (ANR-08-MNP-030) to A.C. We acknowledge M. Tessier-Lavigne (Laboratory of Brain Development and Repair, Rockefeller University) and A.B. Huber (Institute for Developmental Genetics, GSF-Research Center for Environment and Health) for sharing mouse lines. We thank T. Toyofuku (Osaka University) and A. Püschel (Abt. Molekularbiologie, Institut für Allgemeine Zoologie und Genetik, Westfälische Wilhelms-Universität) for sharing plasmids.

AUTHOR CONTRIBUTIONS

C.D.-B. designed and conducted the majority of experiments. A.J. constructed expression vectors and participated in the experiments in **Figure 7**. C.C., F.R., H.N., K.T., K.K. and J.F. contributed to experiments shown in the figures and performed genotyping. Y.Y. provided *Plxna1* embryos and mouse line. Y.K. and Y.E.J. contributed to the binding experiments and purified Slit2C protein. Y.Z. and A.C. provided various constructs and mouse lines and validated various antibodies. A.C. brought scientific input and advice for manuscript preparation. V.C. designed the experimental plan, supervised the project and wrote the manuscript with C.D.-B.

COMPETING FINANCIAL INTERESTS

The authors declare no competing financial interests.

1. Raper, J. & Mason, C. Cellular strategies of axonal pathfinding. *Cold Spring Harb. Perspect. Biol.* **2**, a001933 (2010).
2. Bashaw, G.J. & Klein, R. Signaling from axon guidance receptors. *Cold Spring Harb. Perspect. Biol.* **2**, a001941 (2010).
3. Dickson, B.J. & Gilestro, G.F. Regulation of commissural axon pathfinding by slit and its Robo receptors. *Annu. Rev. Cell Dev. Biol.* **22**, 651–675 (2006).
4. Evans, T.A. & Bashaw, G.J. Axon guidance at the midline: of mice and flies. *Curr. Opin. Neurobiol.* **20**, 79–85 (2010).
5. Nawabi, H. & Castellani, V. Axonal commissures in the central nervous system: how to cross the midline? *Cell. Mol. Life Sci.* **68**, 2539–2553 (2011).
6. Zou, Y., Stoeckli, E., Chen, H. & Tessier-Lavigne, M. Squeezing axons out of the gray matter: a role for slit and semaphorin proteins from midline and ventral spinal cord. *Cell* **102**, 363–375 (2000).
7. Nawabi, H. *et al.* A midline switch of receptor processing regulates commissural axon guidance in vertebrates. *Genes Dev.* **24**, 396–410 (2010).
8. Charoy, C. *et al.* Gdnf activates midline repulsion by Semaphorin3B via NCAM during commissural axon guidance. *Neuron* **75**, 1051–1066 (2012).
9. Kidd, T., Bland, K.S. & Goodman, C.S. Slit is the midline repellent for the robo receptor in *Drosophila*. *Cell* **96**, 785–794 (1999).
10. Kidd, T., Russell, C., Goodman, C.S. & Tear, G. Dosage-sensitive and complementary functions of roundabout and commissureless control axon crossing of the CNS midline. *Neuron* **20**, 25–33 (1998).
11. Seeger, M., Tear, G., Ferres-Marco, D. & Goodman, C.S. Mutations affecting growth cone guidance in *Drosophila*: genes necessary for guidance toward or away from the midline. *Neuron* **10**, 409–426 (1993).
12. Long, H. *et al.* Conserved roles for Slit and Robo proteins in midline commissural axon guidance. *Neuron* **42**, 213–223 (2004).
13. Brose, K. *et al.* Slit proteins bind Robo receptors and have an evolutionarily conserved role in repulsive axon guidance. *Cell* **96**, 795–806 (1999).
14. Chen, J.H., Wen, L., Dupuis, S., Wu, J.Y. & Rao, Y. The N-terminal leucine-rich regions in Slit are sufficient to repel olfactory bulb axons and subventricular zone neurons. *J. Neurosci.* **21**, 1548–1556 (2001).
15. Nguyen Ba-Charvet, K.T. *et al.* Diversity and specificity of actions of Slit2 proteolytic fragments in axon guidance. *J. Neurosci.* **21**, 4281–4289 (2001).
16. Chédotal, A. Slits and their receptors. *Adv. Exp. Med. Biol.* **621**, 65–80 (2007).
17. Jaworski, A., Long, H. & Tessier-Lavigne, M. Collaborative and specialized functions of Robo1 and Robo2 in spinal commissural axon guidance. *J. Neurosci.* **30**, 9445–9453 (2010).
18. Toyofuku, T. *et al.* Dual roles of Sema6D in cardiac morphogenesis through region-specific association of its receptor, Plexin-A1, with off-track and vascular endothelial growth factor receptor type 2. *Genes Dev.* **18**, 435–447 (2004).
19. Chen, Z., Gore, B.B., Long, H., Ma, L. & Tessier-Lavigne, M. Alternative splicing of the Robo3 axon guidance receptor governs the midline switch from attraction to repulsion. *Neuron* **58**, 325–332 (2008).
20. Falk, J. *et al.* Dual functional activity of semaphorin 3B is required for positioning the anterior commissure. *Neuron* **48**, 63–75 (2005).
21. Giordano, S. *et al.* The semaphorin 4D receptor controls invasive growth by coupling with Met. *Nat. Cell Biol.* **4**, 720–724 (2002).
22. Swiercz, J.M., Kuner, R. & Offermanns, S. Plexin-B1/RhoGEF-mediated RhoA activation involves the receptor tyrosine kinase ErbB-2. *J. Cell Biol.* **165**, 869–880 (2004).
23. Mitsui, N. *et al.* Involvement of Fes/Fps tyrosine kinase in semaphorin3A signaling. *EMBO J.* **21**, 3274–3285 (2002).
24. Blom, N., Gammeltoft, S. & Brunak, S. Sequence and structure-based prediction of eukaryotic protein phosphorylation sites. *J. Mol. Biol.* **294**, 1351–1362 (1999).
25. Toyofuku, T. *et al.* FARP2 triggers signals for Sema3A-mediated axonal repulsion. *Nat. Neurosci.* **8**, 1712–1719 (2005).
26. Turner, L.J., Nicholls, S. & Hall, A. The activity of the plexin-A1 receptor is regulated by Rac. *J. Biol. Chem.* **279**, 33199–33205 (2004).
27. Briançon-Marjollet, A. *et al.* Trio mediates netrin-1–induced Rac1 activation in axon outgrowth and guidance. *Mol. Cell. Biol.* **28**, 2314–2323 (2008).
28. Yang, L. & Bashaw, G.J. Son of sevenless directly links the Robo receptor to rac activation to control axon repulsion at the midline. *Neuron* **52**, 595–607 (2006).
29. Vikis, H.G., Li, W. & Guan, K.-L. The plexin-B1/Rac interaction inhibits PAK activation and enhances Sema4D ligand binding. *Genes Dev.* **16**, 836–845 (2002).
30. Kruger, R.P., Aurandt, J. & Guan, K.-L. Semaphorins command cells to move. *Nat. Rev. Mol. Cell Biol.* **6**, 789–800 (2005).
31. Unni, D.K. *et al.* Multiple Slits regulate the development of midline glial populations and the corpus callosum. *Dev. Biol.* **365**, 36–49 (2012).
32. Cho, J.H., Kam, J.W.K. & Cloutier, J.-F. Slits and Robo-2 regulate the coalescence of subsets of olfactory sensory neuron axons within the ventral region of the olfactory bulb. *Dev. Biol.* **371**, 269–279 (2012).
33. Johnson, K.G. *et al.* Axonal heparan sulfate proteoglycans regulate the distribution and efficiency of the repellent slit during midline axon guidance. *Curr. Biol.* **14**, 499–504 (2004).
34. Xiao, T. *et al.* Assembly of lamina-specific neuronal connections by slit bound to type IV collagen. *Cell* **146**, 164–176 (2011).
35. Wright, K.M. *et al.* Dystroglycan organizes axon guidance cue localization and axonal pathfinding. *Neuron* **76**, 931–944 (2012).
36. Philipp, M. *et al.* RabGDI controls axonal midline crossing by regulating Robo1 surface expression. *Neural Dev.* **7**, 36 (2012).
37. Whitford, K.L. *et al.* Regulation of cortical dendrite development by Slit-Robo interactions. *Neuron* **33**, 47–61 (2002).
38. Mehlen, P., Delloye-Bourgeois, C. & Chédotal, A. Novel roles for Slits and netrins: axon guidance cues as anticancer targets? *Nat. Rev. Cancer* **11**, 188–197 (2011).
39. Gu, C. & Giraudo, E. The role of semaphorins and their receptors in vascular development and cancer. *Exp. Cell Res.* **319**, 1306–1316 (2013).
40. Marquardt, T. *et al.* Coexpressed EphA receptors and ephrin-A ligands mediate opposing actions on growth cone navigation from distinct membrane domains. *Cell* **121**, 127–139 (2005).

ONLINE METHODS

Genotyping of mouse lines. Mouse tissue samples were lysed in 50 mM NaOH for 20 min at 95 °C. Genotyping of *Plxna1*, *Sema3B*, *Robo1/2* and *Slit1/2/3* mouse lines was performed as described in refs. 19,20 and 41–43. The *Nrp2* mouse line was a gift of A.B. Huber (Institute of Developmental Genetics, Germany) and was genotyped as described in ref. 44. This work was conducted in accordance with ethical rules of the European Community and French research ethical guidelines.

Plasmids, siRNAs and recombinant proteins. Constructs encoding full-length, extracellular and cytoplasmic mouse PlexinA1 were kind gifts of T. Toyofuku, Osaka University. Chick PlexinA1-GFP in the pCAGGS vector was a gift of Y.Y., Cincinnati Children's Hospital Medical Center. Vectors encoding Myc-tagged human Slit1-FL, Slit2-FL, the Slit2 N-terminal fragment (SlitN), the Slit2 C-terminal fragment (Slit2C) and Slit2U were described previously in ref. 15. The Slit2N and Slit2C sequences are fused in the N terminus to the human AP sequence. The Slit1C sequence was fused to a Myc tag in the C terminus and cloned in the pcDNA3.1 vector. The rat Robo2 sequence was cloned in the pcDNA3.1-V5 vector (Invitrogen). The vector encoding mouse Nrp2 was a kind gift of A. Püschel and was described in ref. 45. Mouse-specific PlexinA1 siRNA and scrambled siRNA were purchased from Sigma. GDNF and Slit2N recombinant proteins were purchased from Sigma and R&D Systems, respectively. Recombinant Slit2C was produced as described previously[46]. Briefly, samples were purified from dialyzed medium by immobilized metal-affinity and size-exclusion chromatography using fast protein liquid chromatography (FPLC) coupled with a HiLoad Superdex 200 pg column from GE Healthcare Life Sciences.

DiI staining on spinal cord open-book preparations. Spinal cords from E12.5 embryos were dissected in open-book conformation and fixed in 4% paraformaldehyde (PFA) for 18 h. DiI crystals (Invitrogen) were inserted in the most dorsal part of one hemicord to achieve anterograde labeling of commissural fibers. Axon trajectories were analyzed 24 h later with a microscope equipped with a spinning disk module (Olympus X80). For each DiI crystal, several types of phenotypes can be observed among the labeled fibers. Each class represents the percentage of DiI crystals showing the phenotype over the total number of observed DiI crystals. Classes of phenotypes were assessed independently from each other and range from 0% to 100%.

Culture assays. FP conditioned medium was prepared as described previously in refs. 7,8. Collapse assays were performed as described previously[7,8]. When required, dissociated neurons were transfected after 24 h of culture using Lipofectamine 2000 reagent (Invitrogen) with either siRNAs (20 pmol per coverslip) or plasmids (1 µg per coverslip). Growth cone collapse was quantified as described in ref. 20. Cocultures of HEK293T cell aggregates and dorsal spinal cord explants were performed as described in ref. 8 and analyzed as described previously[20]. Briefly, a qualitative guidance index was attributed to each explant according to the degree of repulsive (negative values) or attractive (positive values) effects, ranging from −2 to +2.

Chick *in ovo* electroporation. *In ovo* electroporation of chick embryos (*Gallus gallus*; EARL Morizeau, Dangers, France) was performed as described previously[47,48].

Immunofluorescent labeling. Immunofluorescent labeling was performed as described in ref. 8. The following primary antibodies were applied to cryosections or coverslips overnight at 4 °C: anti-Robo2 (1/100, Abcam, ab64148), anti-Robo3 (1/100, R&D, AF3076), anti-Myc (1/150, Sigma, M4339), anti-Slit1 (1/200, Abnova, PAB20356), anti-PlexinA1 (1/100, Abcam, ab23391), anti-PlexinA3 (1/100, Santa Cruz, sc-25641), anti-Flag (1/150, Sigma, F4725) and anti-VSV (1/500, Sigma, V4888). Alexa 488, Alexa 555 (1/500, Invitrogen) and Fluoroprobe 546 (1/400) were used as secondary antibodies. The Slit1 antibody was validated with WT and *Slit1*$^{-/-}$ embryonic sections and has also been validated by Antibodypedia.

Coimmunoprecipitation and western blot experiments. *In vitro* and *in vivo* coimmunoprecipitation experiments were performed as described previously[49].

For phosphorylation and Rac1 or ERK activation analyses, COS7 cells and HEK293T cells, respectively, transfected with PlexinA1 were starved for 2 h in OptiMEM medium (Gibco) and then incubated with supernatants from HEK293T cells transfected with Slit1-FL, Slit2-FL, Slit2N, Slit2C or Slit2U constructs. For the Rac1 activation analysis, cell lysates were incubated with glutathione *S*-transferase (GST) fusion protein, corresponding to the p21-binding domain (PBD, residues 67–150) of human PAK-1 bound to glutathione agarose (Millipore), allowing for coprecipitation of GTP-bound Rac1.

Western blot analysis was performed using the following primary antibodies: anti-Flag (1/1,000, Sigma, F4725), anti-Myc (1/1,000, Sigma, M4339), anti-HA (1/5,000, Sigma, H6908) anti-PlexinA1 (1/500, Abcam, ab32960 for western blotting (WB); sc-25639 for IP), anti-Slit1 (1/1,000, Abnova, PAB20356), anti-Slit2C (1/1,000, Epitomics, 2864-1), anti-Slit2N (1/2,000, GeneTex, GTX118220, validated by Antibodypedia), anti-Robo1 (1/500, Abcam, ab85312), anti-Robo2 (1/500, Abcam, ab64158), anti-Nrp2 (1/1,000, R&D, AF567), anti-pTyr (1/1,000, Upstate, 05-321), anti-Rac1 (1/1,000, BD Transduction Laboratories, 610650), anti-ERK (1/1,000, Santa Cruz, sc-93), anti-pERK (1/1,000, Santa Cruz, sc-7383) and anti–β-actin (1/5,000, Sigma, A5316). Antibodies to PlexinA1 and Nrp2 were validated in ref. 7. Western blot validation of Slit2C, Robo1, Robo2 and Nrp2 antibodies using tissue lysates from WT and the corresponding knockout embryos are shown in **Supplementary Figure 10**. Western blot quantification was performed using Image Lab4.0 software (Bio-Rad) on three independent experiments.

Binding experiments. *Binding experiments on intact cells.* 2.5×10^4 COS7 cells plated on glass coverslips were transiently transfected with either PlexinA1-GFP, Robo2 or Neuropilin2 constructs. 48 h later, the COS7 cells were incubated with PBS supplemented with 10% fetal bovine serum for 20 min at room temperature. Concentrated supernatants from HEK293T cells expressing Myc-tagged Sema3C, Slit2N, Slit2C or Slit2-LRR2 constructs were then applied to the COS7 cells for 2 h at 10 °C. After washing three times in PBS, COS7 cells were fixed in 4% PFA for 20 min at room temperature. Immunofluorescent labeling of Myc-tagged soluble proteins and transmembrane receptors was then performed.

Quantitative binding experiments. 4.5×10^4 COS7 cells were plated in 24-well plates and transfected with either PlexinA1, Robo2, PlexinA2, PlexinA3, PlexinA4 or PlexinB1 constructs. 48 h later, the COS7 cells were incubated with DMEM supplemented with 10% fetal bovine serum and 1 µg/ml heparin for 10 min at room temperature. Serial dilutions of previously dosed supernatants from HEK293T cells expressing AP-tagged Slit2N or Slit2C were then applied to the COS7 cells for 2 h at 37 °C. Cells were then washed, and AP activity was measured in cell lysates using the Alkaline Phosphatase Assay Kit (Abcam ab83369). Binding curves were fitted using the Hill equation, and corresponding K_d values were calculated with Prism 6 software (GraphPad).

Samples sizes. No statistical methods were used to predetermine sample sizes, but our sample sizes are similar to those reported in refs. 7,8.

Blinding. Data collection and analyses for *ex vivo* experiments (DiI staining, collapse assays and spinal cord explant coculture experiments) were performed blinded regarding the treatments applied and/or embryos genotypes. Data collection and analyses were not performed blinded to the conditions of the *in vitro* experiments.

Randomization. For *ex vivo* experiments, embryos were collected and processed randomly and assigned to experimental groups a posteriori according to their genotypes. For the *in vitro* experiments, experimental points were treated randomly. More precisely, for the phosphorylation assay, cells of each condition were blocked on ice simultaneously and collected randomly in lysis buffer to overcome experimental bias due to phosphorylation instability.

Statistical analyses. The statistical tests used for data analyses are mentioned in each figure legend. Normality was tested for each data set using Sigma Stat Software. Nonparametric tests were used for data sets showing non-normal distribution or unequal variances. In every case, statistical tests were performed as two sided.

A **Supplementary Methods** checklist is available.

41. Yoshida, Y., Han, B., Mendelsohn, M. & Jessell, T.M. PlexinA1 signaling directs the segregation of proprioceptive sensory axons in the developing spinal cord. *Neuron* **52**, 775–788 (2006).

doi:10.1038/nn.3893

42. Plump, A.S. *et al.* Slit1 and Slit2 cooperate to prevent premature midline crossing of retinal axons in the mouse visual system. *Neuron* **33**, 219–232 (2002).
43. Yuan, W. *et al.* A genetic model for a central (septum transversum) congenital diaphragmatic hernia in mice lacking Slit3. *Proc. Natl. Acad. Sci. USA* **100**, 5217–5222 (2003).
44. Giger, R.J. *et al.* Neuropilin-2 is required *in vivo* for selective axon guidance responses to secreted semaphorins. *Neuron* **25**, 29–41 (2000).
45. Rohm, B., Ottemeyer, A., Lohrum, M. & Püschel, A.W. Plexin/neuropilin complexes mediate repulsion by the axonal guidance signal semaphorin 3A. *Mech. Dev.* **93**, 95–104 (2000).
46. Zhao, Y. *et al.* Automation of large scale transient protein expression in mammalian cells. *J. Struct. Biol.* **175**, 209–215 (2011).
47. Creuzet, S., Couly, G., Vincent, C. & Le Douarin, N.M. Negative effect of Hox gene expression on the development of the neural crest-derived facial skeleton. *Development* **129**, 4301–4313 (2002).
48. Blank, M.C., Chizhikov, V. & Millen, K.J. *In ovo* electroporations of HH stage 10 chicken embryos. *J. Vis. Exp.* **408** (2007).
49. Bechara, A. *et al.* FAK-MAPK–dependent adhesion disassembly downstream of L1 contributes to semaphorin3A-induced collapse. *EMBO J.* **27**, 1549–1562 (2008).